Pr^{10+} as a candidate for a high-accuracy optical clock for tests of fundamental physics

S. G. Porsev,[1] C. Cheung,[1] M. S. Safronova,[1] H. Bekker,[2] N.-H. Rehbehn,[3] J. R. Crespo López-Urrutia,[3] and S. M. Brewer[4]

[1]*Department of Physics and Astronomy, University of Delaware, Newark, Delaware 19716, USA*
[2]*Helmholtz-Institut, GSI Helmholtzzentrum für Schwerionenforschung, 55128 Mainz, Germany*
[3]*Max-Planck-Institut für Kernphysik, 69117 Heidelberg, Germany*
[4]*Department of Physics, Colorado State University, Fort Collins, Colorado 80523, USA*

(Received 24 July 2024; accepted 4 October 2024; published 22 October 2024)

We propose In-like Pr^{10+} as a candidate for the development of a high-accuracy optical clock with high sensitivity to a time variation of the fine-structure constant, $\dot{\alpha}/\alpha$, as well as favorable experimental systematics. We calculate its low-lying energy levels by combining the configuration interaction and the coupled cluster method, achieving uncertainties as low as 0.1%, and improving previous work. We benchmark these results by comparing our calculations for the $|5s^25p\ ^2P_{1/2}\rangle \rightarrow |5s^25p\ ^2P_{3/2}\rangle$ transition in Pr^{10+} with a dedicated measurement and for Pr^{9+} with a recent experiment, respectively. In addition, we report calculated hyperfine-structure constants for the clock and logic states in Pr^{10+}.

DOI: 10.1103/PhysRevA.110.042823

I. INTRODUCTION

Optical atomic clocks belong to the most promising platforms for low-energy fundamental physics tests [1]. Their frequency ratios were used for laboratory-based investigations of general relativity [2–4], searches for signatures of ultralight scalar dark matter [3,5], and tests for possible violations of local Lorentz invariance and local position invariance [6,7]. They also yield constraints on a possible time variation of fundamental constants, such as the proton-to-electron mass ratio (m_p/m_e) or the fine-structure constant ($\dot{\alpha}/\alpha$) [8–11].

Over the last few decades, optical clock development has focused on trapped, singly charged ions (i.e., Al^+, Yb^+) or ensembles of neutral atoms (i.e., Sr, Yb) [12]. More recently, clocks based on laser-accessible transitions in highly charged ions (HCIs) or the nuclear clock transition in ^{229}Th have been proposed to enhance sensitivity to signatures of new physics [1,13,14]. In particular, strong relativistic effects in HCIs make their optical transitions the most sensitive to $\dot{\alpha}/\alpha$ [15–20] (for a review, see Ref. [13]) in atomic systems. Hyperfine transitions in heavy hydrogen-like [21] and Li-like [22] ions were also proposed for such studies, since they are extreme examples of relativistic effects on the binding energy of the electron and are accessible by lasers. The high charge state also largely suppresses detrimental systematic frequency shifts due to perturbations such as ac Stark shifts from blackbody radiation (BBR), as required for the most stringent clock comparisons [5,11].

In this work, we propose a narrow linewidth transition in Pr^{10+} to develop a high-accuracy optical clock for fundamental physics tests and predict its value. Both Pr^{10+} and Pr^{9+} possess α-sensitive "clock" transitions, as well as laser-accessible "logic" transitions that are well suited for state readout using the quantum-logic spectroscopy (QLS) technique [23]. We consider the experimental feasibility of a quantum-logic clock based on Pr^{10+} and calculate crucial properties for this purpose, such as hyperfine coefficients A and B. We also estimate the expected leading systematic uncertainties and frequency instability and evaluate the possibility of improving current bounds on $\dot{\alpha}/\alpha$ by comparing the frequency of our proposed clock with the one based on the electric-octupole ($E3$) transition in Yb^+ [9,24].

To validate our predictions, we also measured the Pr^{10+} $|5s^25p\ ^2P_{1/2}\rangle \rightarrow |5s^25p\ ^2P_{3/2}\rangle$ $M1$ transition with an electron beam ion trap (EBIT) and found excellent agreement. Our present Pr^{10+} theory results also match well with previous calculations but achieve higher precision than those, which is critical for upcoming experimental searches for the ultranarrow clock transition [18]. Moreover, we also calculate the level energies for the Pr^{9+} ion energies, which also agree within uncertainties with an earlier measurement [25].

These theoretical benchmarks are important for other proposed clocks based on Cf^{15+} and Cf^{17+} [26]. The uncertainty of predictions for clock transitions in such open-shell ions is large because of the effect of triple excitations in the coupled cluster part of the computation. We now improve the treatment of these corrections by including core-triple excitations. The agreement of the Pr^{9+} and Pr^{10+} experiments with the present calculations strengthens our confidence in this method for future predictions of Cf.

II. ATOMIC STRUCTURE CALCULATIONS

We use a hybrid approach that combines the configuration interaction (CI) and coupled-cluster (all-order) method. The CI wave function is obtained as a linear combination of all distinct states of a given angular momentum J and parity:

$$\Psi_J = \sum_i c_i \Phi_i. \tag{1}$$

Low-lying energies and wave functions are determined by diagonalizing the effective Hamiltonian

$$H^{\rm eff} = H_1 + H_2, \tag{2}$$

where H_1 and H_2 represent the one- and two-electron parts of the Hamiltonian, respectively. The CI + all-order approach allows one to incorporate core excitations in the CI method by including dominant core-core and core-valence correlation corrections into the effective Hamiltonian for all orders. We thus include in the one-electron part H_1 a correlation potential Σ_1, which accounts for its core-valence correlations:

$$H_1 \to H_1 + \Sigma_1, \tag{3}$$

while also including in the two-electron part H_2 the respective core-valence interactions:

$$H_2 \to H_2 + \Sigma_2. \tag{4}$$

A detailed description of the CI + all-order method and all formulas is given in Ref. [27]. We use the parallel CI package developed in Ref. [28] for all calculations.

We begin our study with Sn-like Pr^{9+}, where experimental data are available [25]. To evaluate the uncertainties of our results, we performed several calculations to separate the contributions of higher-order correlations, higher partial waves, triple excitations, and quantum-electrodynamical (QED) contributions. We then used the same approach to study Pr^{10+}, for which no experimental data were available before this work.

We consider both Pr^{9+} and Pr^{10+} ions as atomic systems with $[1s^2, \ldots, 4d^{10}]$ closed core shells and open $5s$, $5p$, $5d$, $6s$, $6p$, and $4f$ valence shells. We used a complete set of Dirac-Hartree-Fock wave functions on a radial grid generated using B splines constrained to a spherical cavity of radius $R = 20$ a.u. The basis set is constructed using 40 splines of order seven. The Breit interaction is included in the stage of constructing the basis set. We treat Pr^{9+} as a four-valent system and start with all possible single and double excitations to any orbital up to $22spdfg$ from the $5s^2 5p^2$ and $5s^2\,5p4f$ even configurations (in the following, we leave out the $5s^2$ from the configuration designations for brevity). Here, $22spdfg$ indicates that excitations to all orbitals up to $n = 22$ are included for the $spdfg$ partial waves.

In Table I, we list the energies obtained from increasing sets of configurations (from $22spdfg$ to $30spdfg$) and show their convergence. The energy differences between $22spdfg$ and $26spdfg$ do not exceed 74 cm^{-1}, while the largest difference between $26spdfg$ and $30spdfg$ is only about 3 cm^{-1}. This clear convergence of CI allows us to use the set of configurations $22spdfg$ for subsequent calculations, which is sufficiently complete but does not make the calculations too time-consuming.

The contributions to the excitation energies of Pr^{9+} from other correlation effects are listed in Table II. The results are compared with the experimental data from Ref. [25]. We added corrections due to three-electron excitations from the main configurations and allowed single and double excitations only from the $5s^2 4f^2$ configuration, since including additional main configurations had a negligible effect. The calculated corrections, listed in columns "triples" and "$4f^2$" of Table II, are relatively small and partially cancel each other. The energy differences between $22spdfg$ and $30spdfg$ are given in the column labeled "(23–30)$spdfg$." We then performed calculations for $30spdfgh$ and $30spdfghi$, including excitations from the main configurations to the $6h$–$30h$ and $7i$–$30i$ orbitals, and list the respective corrections in the columns labeled "(6–30)h" and "(7–30)i."

TABLE I. Energy corrections for Pr^{9+} calculated with increasing CI space size (all energies are given in cm^{-1}) for the $n\,spdfg$ sets of configurations, where n is the largest principal quantum number for each included partial wave.

Term	$22spdfg$	$26spdfg$	$30spdfg$
$5p^2\ {}^3P_0$	0	0	0
$5p4f\ {}^3G_3$	22815	−66	−2
$5p4f\ {}^3F_2$	24915	−66	−3
$5p4f\ {}^3D_3$	27956	−70	−2
$5p^2\ {}^3P_1$	28462	7	0
$5p4f\ {}^3G_4$	30288	−74	−3
$5p^2\ {}^3D_2$	36453	−15	−1
$5p4f\ {}^3F_3$	56151	−63	−2
$5p4f\ {}^3F_4$	59869	−68	−2
$5p^2\ {}^3F_2$	62748	−54	−2
$5p4f\ {}^3G_5$	65030	−65	−2
$5p4f\ {}^1F_3$	64843	−73	−2
$5p^2\ {}^3P_2$	67777	−45	−2
$5p4f\ {}^3D_1$	68481	−71	−3

Using the expressions for the cluster amplitudes derived in Ref. [29], we included the nonlinear (NL) terms and triple excitations into the formalism of the CI + all-order method developed in Ref. [27]. The total corrections for these terms are presented in the column labeled "NLTr." Following Refs. [30] and [31], respectively, we included QED corrections and three-electron interaction (TEI) corrections. They are given in the columns "QED" and "TEI."

Additionally, we explored the contributions of higher partial waves in the all-order expansion. Partial waves with $l_{max} = 6$ are included in every summation in all-order terms for each of the calculations. To explore the role of higher partial waves, we also performed a complete all-order calculation with $l_{max} = 7$ and $l_{max} = 8$ and found that the inclusion of partial waves with $l > 6$ is very important for an accurate description of the $5p4f$ states. We extrapolate the contribution $l > 6$ following the method described in Ref. [32]. We estimate the effect of higher partial waves on Pr^{9+} as the difference between the results obtained for $l_{max} = 8$ and $l_{max} = 6$ to which we added the difference between the results obtained for $l_{max} = 8$ and $l_{max} = 7$. This contribution is labeled "Extrap." in Table II.

The comparison of theoretical and experimental excitation energies for Pr^{9+} (the last column, "Diff.", in Table II) shows that the difference does not exceed 70 cm^{-1} for most states belonging to the $5p4f$ configuration. For the difference between the fine-structure states $5p^2\ {}^3P_0$ and $5p^2\ {}^3P_1$, the theory differs from the experiment by only 12 cm^{-1}. This remarkable agreement shows the predictive power of this approach for Pr^{10+}. Although the effect of triple excitations is even larger in Cf ions, we expect that the inclusion of core triple excitations will allow us to improve the accuracy of the predicted clock wavelength from that of Ref. [26].

TABLE II. Contributions to the excitation energies of Pr^{9+} (in cm^{-1}) from different correlation effects (all energies are given in cm^{-1}). The final excitation energies (given in the column labeled "Final") are calculated by adding the corrections (see the main text) listed in columns 3–11 to the base result $22spdfg$. The experimental values of Ref. [25] are shown in the column labeled "Expt. [25]." The differences between the final theoretical and experimental results are given (in cm^{-1}) in the column "Diff."

Term [25]	$22spdfg$	Triples[a]	$4f^2$	$(23–30)spdfg$	$(6–30)h$	$(7–30)i$	NLTr	QED	TEI	Extrap.	Final	Expt. [25]	Diff.
$5p4f\ ^3G_3$	22815	26	−4	−69	−217	−41	893	−199	−107	−1065	22032	22101	−69
$5p4f\ ^3F_2$	24915	18	−4	−68	−191	−35	631	−152	219	−885	24448	24494	−46
$5p4f\ ^3D_3$	27956	21	−6	−72	−222	−42	840	−123	18	−1058	27310	27287	23
$5p^2\ ^3P_1$	28462	18	8	7	29	13	−69	61	37	7	28573	28561	12
$5p4f\ ^3G_4$	30288	20	−8	−77	−278	−59	828	−124	−258	−1066	29266	29231	35
$5p^2\ ^3D_2$	36453	4	−2	−15	−56	−11	181	4	113	−234	36436	36407	29
$5p4f\ ^3F_3$	56151	23	−7	−66	−194	−36	832	−144	178	−1057	55681	55662	19
$5p4f\ ^3F_4$	59869	22	−8	−70	−210	−40	794	−104	16	−1054	59215	59185	30
$5p^2\ ^3F_2$[b]	62748	12	−6	−56	−174	−30	434	−73	−2	−753	62101	62182	−81
$5p4f\ ^3G_5$	65030	27	−3	−67	−239	−46	737	−69	−483	−1045	63842	63924	−82
$5p4f\ ^1F_3$[c]	64843	17	−7	−76	−238	−43	720	−81	−190	−1047	63898	63964	−66
$5p^2\ ^3P_2$[d]	67777	7	−7	−47	−142	−22	347	−24	−100	−614	67175	67291	−116
$5p4f\ ^3D_1$	68481	16	−4	−74	−267	−48	694	−144	−542	−1049	67063	67309	−246

[a]These terms were calculated for $12spdfg$.
[b]This term must have a typo in Ref. [25] because the $5p^2$ configuration cannot have $L = 3$. We determined it to be $5p4f\ ^3D_2$.
[c]In this work, we determined this term to be $^3D_3$.
[d]We determined this term to be $^3D_2$ with the following weights of the two main configurations: 57% $5p4f$ and 38% $5p^2$.

A. Pr^{10+} energies

Our treatment of Pr^{10+} as a trivalent system starts with all possible single and double excitations to any orbital up to $26spdfg$ from the $5s^25p$ and $5s^24f$ odd main configurations. A simplified energy-level diagram highlighting the transitions of interest is shown in Fig. 1.

In Table III, we list the contributions to the Pr^{10+} energies from different correlation effects. Excitations from additional main configurations (AMC) $5p^24f$, $5p^3$, $5s5p5d$, $5s6s4f$, and $5s5p6s$ give a small contribution to the excitation energies. They are presented in a column labeled "AMC" in Table III. By performing the calculation for $30spdfg$, we determined contributions from configurations obtained by excitations to 27–30 $spdfg$ shells (labeled "$(27–30)spdfg$"). All other contributions to the excitation energies listed in the table are analogous to those for Pr^{9+} described above.

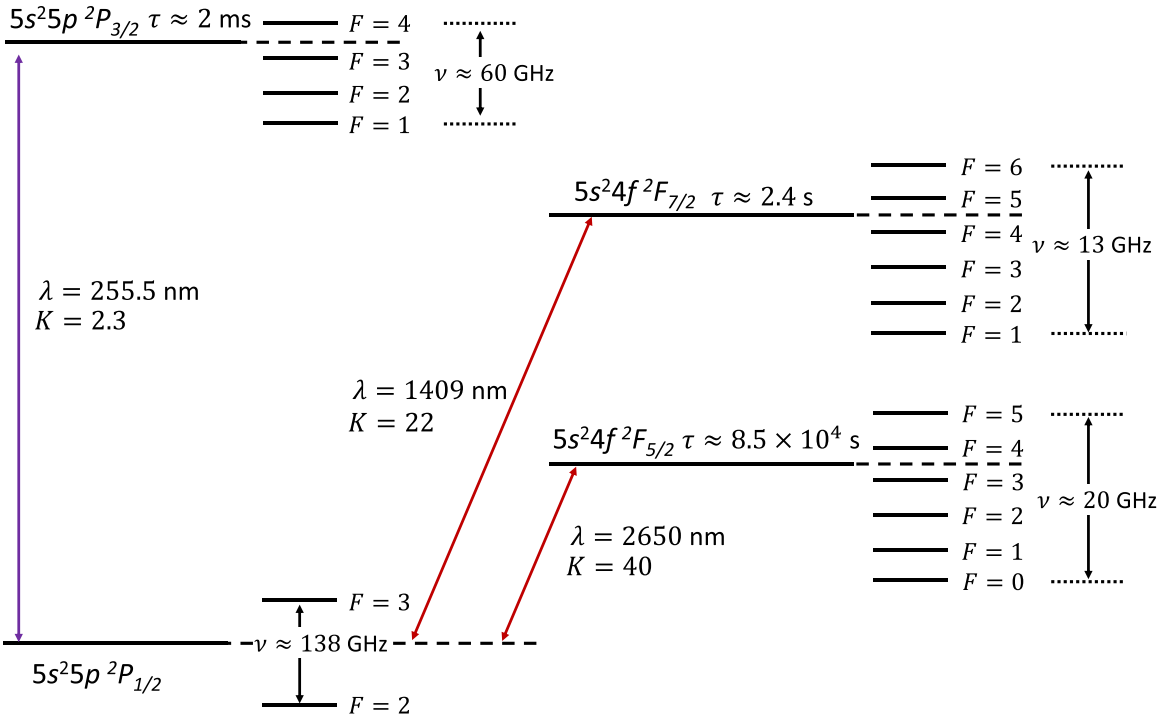

FIG. 1. Energy levels, radiative lifetimes, and hyperfine-structure of the lowest states in $^{141}Pr^{10+}$, with nuclear spin, $I = 5/2$.

TABLE III. Contributions to the excitation energies of Pr^{10+} (in cm^{-1}) from different correlation effects. The final excitation energies (given in the column labeled "Final") are calculated by adding the corrections listed in columns 3–11 to the base result $26spdfg$. The theoretical results of Ref. [18] are presented for comparison. The uncertainties are given in parentheses.

Term	$26spdfg$	Triples[a]	AMC[b]	$(27–30)spdfg$	$(6–30)h$	$(7–30)i$	NLTr	QED	TEI	Extrap.	Final	Ref. [18]
$4f_{5/2}$	4372	2	2	−2	−178	−43	845	−98	−37	−1090	3773(70)	3702(200)
$4f_{7/2}$	7734	2	2	−2	−180	−43	810	−97	−43	−1083	7099(70)	7031(200)
$5p_{3/2}$	39139	0	0	0	5	2	−69	50	7	7	39140(15)	39141(40)

[a]These terms were calculated for *12spdfg*,
[b]Contribution from electron excitations from additional main configurations $5p^24f$, $5p^3$, *5s5p5d*, *5s6s4f*, and *5s5p6s*.

Based on the results for the excitation energies of Pr^{9+} and considering that the calculation for Pr^{10+} was performed similarly, producing comparable precision, we assign uncertainties to the energies of the excited states. The final values with their uncertainties are given in Table III in the column "Final."

B. Hyperfine-structure constants

We also calculated the magnetic-dipole and electric-quadrupole hyperfine-structure (hfs) constants A and B of the four lowest-lying states. For $^{141}Pr^{10+}$, the nuclear spin is $I = 5/2$ and the nuclear magnetic-dipole and electric-quadrupole moments are $\mu/\mu_N = 4.2754(5)$ (where μ_N is the nuclear magneton) and $Q = -0.077(7)$ b, respectively [33].

The results obtained for the $[26spdfg]$ set of configurations are summarized in Table IV. In the third column, we present the results for the g factors of the states obtained in the CI + all-order approximation. In the fourth, we give the results obtained at the CI + MBPT stage when the core-valence correlations are included in the second order of the perturbation theory. CI + all-order results that include higher-order core-valence correlations are displayed in the column labeled "CI + All." Finally, we included random-phase approximation (RPA) corrections; the results are listed in the column labeled "CI + All + RPA." We use these results to arrive at the final values listed in column "Final."

Based on the difference between the CI + all-order and CI + MBPT results, we determine the uncertainties for the constants A. For the constants B, the difference between the CI + all-order and CI + MBPT is small, while the RPA corrections change the values of $B(4f_{5/2,7/2})$ by more than 20%. Here, we do not take into account corrections to the hyperfine operator beyond RPA, such as the core Brueckner, structural radiation, two-particle corrections, and normalization (see Ref. [34] for more details), which can affect the values of the constants B noticeably. For this reason, we consider their final values as estimates sufficiently accurate for our present purpose of analyzing experimental measurement and assessing proposed clock accuracy.

TABLE IV. Calculated g factor and hfs constants A and B (in MHz). The CI + MBPT and CI + all-order values are listed in the columns labeled "CI + MBPT" and "CI + All," respectively. The values including the RPA corrections, are listed in the column labeled "CI + All + RPA." The final values are given in the column labeled "Final." Uncertainties are given in parentheses.

	g	CI + MBPT	CI + All	CI + All + RPA	Final
$A\ 5p_{1/2}$	0.666	46318	42722	46070	46 100(3600)
$A\ 4f_{5/2}$	0.856	1690	1277	1313	1300(400)
$A\ 4f_{7/2}$	1.142	773	965	675	670(190)
$A\ 5p_{3/2}$	1.333	7153	5736	6596	6600(1400)
$B\ 4f_{5/2}$		−69	−67	−84	−85
$B\ 4f_{7/2}$		−79	−77	−98	−100
$B\ 5p_{3/2}$		−571	−528	−586	−585

C. Electric-quadrupole moments and polarizabilities

We also calculate the electric-quadrupole moments and polarizabilities of the ground and excited logic and clock states shown in Fig. 1. The quadrupole moment Θ of an atomic state is given by

$$\Theta = 2\langle J, M = J|Q_0|J, M = J\rangle = 2\sqrt{\frac{J(2J-1)}{(2J+3)(J+1)(2J+1)}}\langle J||Q||J\rangle, \quad (5)$$

where $\langle J||Q||J\rangle$ is the reduced matrix element of the electric-quadrupole operator.

The static polarizability α_{JM} of a $|JM\rangle$ state can be expressed as a sum over unperturbed intermediate states:

$$\alpha_{JM} = 2\sum_n \frac{|\langle JM|D_z|J_nM\rangle|^2}{E_n - E_J}, \quad (6)$$

where $\mathbf{D}$ is an electric dipole moment operator, and E_J and E_n are the energy of the state $|JM\rangle$ and an intermediate state $|J_nM\rangle$, respectively.

The results are summarized in Table V. The values of the static polarizabilities calculated at $M = 1/2$ are displayed in the second row. The third row shows the differential polarizabilities between the excited and ground states. The electric-quadrupole moments in ea_B^2, where e is the elementary charge and a_B is the Bohr radius, are given in the fourth row.

TABLE V. Electric-quadrupole moments Θ (in ea_B^2) and polarizabilities (in a.u.) of the ground and excited logic and clock states.

Term	$\alpha_{JM=1/2}$	$\Delta\alpha$	Θ
$5p_{1/2}$	1.72		
$4f_{5/2}$	1.77	0.05	−0.34
$4f_{7/2}$	1.77	0.05	−0.41
$5p_{3/2}$	1.65	−0.07	−0.87

III. Pr^{10+} MEASUREMENTS

To support this work, spectroscopic measurements of the $|5s^2 5p\ ^2P_{1/2}\rangle \rightarrow |5s^2 5p\ ^2P_{3/2}\rangle$ transitions of Pr^{10+} were made (as for Pr^{9+}) with the Heidelberg EBIT (HD-EBIT). It produces HCI by electron-impact ionization with a 3.8 mA electron beam accelerated by a potential of 172 V and focused in an 8 T magnetic field [35]. Praseodymium ions were prepared by injecting an organometallic compound (CAS number 15492-48-5) into the EBIT from a cell. By heating it to 120 °C, a pressure of 6×10^{-8} mbar was established in the second stage of a differential pumping system, generating a tenuous molecular beam that crosses the electron beam at the center of the trap and is dissociated by it, freeing Pr atoms that are immediately ionized by the beam. The produced ions are then trapped, the trap depth being made sufficiently shallow by applying potentials to the drift tubes such that light ions of carbon, oxygen, and hydrogen (resulting from the dissociation of the compound) evaporate from the EBIT, leaving a rather pure ensemble of the much heavier ions of Pr, as pioneered in Refs. [36,37]. By tuning the depth of the trap and regularly ejecting the contents of the trap, which tends to accumulate contaminant ions from the cathode materials Ba and W over timescales of minutes, we ensured that Pr^{10+} was the dominant species in the trap at nearly all times.

Continuous electron-impact excitation of Pr^{10+} and subsequent decays generated fluorescence light which was focused on the entrance slit of a grating spectrometer using four lenses and three mirrors. The 2-m focal length spectrometer was fitted with a 3600 lines/mm grating. By operating in third diffraction order, a linear dispersion of 0.9 pm/pixel at 255 nm was achieved [38] in the focal plane where the Peltier-cooled CCD camera is installed. A total of 31 Pr^{10+} spectra were recorded for 1 hour each. These were interspersed with eight spectra obtained without injection of Pr for background subtraction. Calibration spectra were obtained before each Pr^{10+} measurement from a Fe-Mn-Cu-Ne hollow cathode lamp that illuminates a movable diffuse reflector at an intermediate focus of the imaging system. The integrated total Pr^{10+} spectrum and a sample calibration spectrum are shown in Fig. 2. Although Pr^{10+} can be easily produced in compact room-temperature EBITs, the strong magnetic field (up to 8 T, in this case, 5.77 T) of the HD-EBIT yields large Zeeman splittings of the observed transitions, which can be resolved despite Doppler broadening caused by temperatures of the trapped ions here on the order of 10^5 K. This allows for unambiguous identification of lines or, conversely, the determination of g factors and hfs constants.

In the present case, the hyperfine interaction is of similar magnitude as the Zeeman one, so the Breit-Rabi formalism has to be applied. We construct the Hamiltonian on the F, m_F basis relying on the g factors and the hfs A constants from Table IV and determine the eigenvalues and eigenvectors. These are used to model the lineshape, which is fit to the data as in Ref. [39]. The result for the transition energy is 39 122.234(13) cm^{-1}, where the 1σ uncertainty is mainly due to calibration uncertainties. The only other free fit parameters were a Gaussian width common to all Zeeman components

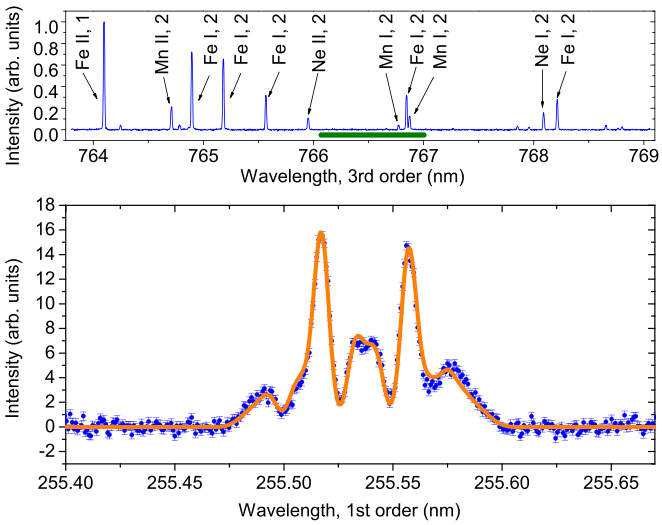

FIG. 2. (top) Spectrum of the Fe-Mn-Cu-Ne calibration lamp. The identified species are labeled, with the second number indicating the diffraction order in which each line appears. The green horizontal line indicates the range displayed in the bottom graph. (bottom) Measured spectrum of the $^2P_{1/2}$-$^2P_{3/2}$ Pr^{10+} transition from 31 hours of exposures (blue) and fit (orange) used to determine the transition energy.

and the ratio between the grating efficiency for s and p polarization due to the Zeeman effect. This measured transition energy is in good agreement with the theoretical prediction of 39 140(15) cm^{-1} listed in Table III.

IV. OPTICAL CLOCK CONSIDERATIONS

Here, we consider the experimental feasibility of developing an optical clock based on Pr^{10+}. Both clock transitions, $|^2P_{1/2}\rangle \rightarrow |^2F_{7/2}\rangle$ and $|^2P_{1/2}\rangle \rightarrow |^2F_{5/2}\rangle$, offer increased sensitivity to possible time-variation of the fine-structure constant $(\dot{\alpha}/\alpha)$ and better systematics than current state-of-the-art ion clocks [11,40]. For technical considerations related to laser performance and frequency instability, we focus on the $|^2P_{1/2}\rangle \rightarrow |^2F_{7/2}\rangle$ transition, which is predicted to have a wavelength of $\lambda = 1409$ nm. Due to the relatively low ionization energy of ≈162 eV, Pr^{10+} has also recently been produced in a compact EBIT using a laser ablation loading scheme [41]. The high ion temperature inside an EBIT precludes clock operation inside it. To this end, sympathetic cooling has to be performed in a separate radio frequency (rf) trap [42], to which the HCI has to be transferred, in this case a single Pr^{10+} ion. The lack of a laser-accessible cooling and readout transition requires co-trapping of this ion with Be^+ to cool it to a temperature of ≈1 mK, where QLS will be used for state readout [23]. When the ions are transferred to the rf trap, their charge state can be confirmed by measuring the motional frequencies of the Be^+/Pr^{10+} ion crystal. Depending on the trapping conditions of the EBIT, the transferred Pr^{10+} ion can be in the ground electronic state or in one of the excited logic or clock states. Based on a collisional-radiative model of the EBIT plasma, a few seconds after ion transfer to the rf trap it will be found in the ground electronic state roughly 50% of the time. Depending on which state the ion is in, clock operation

can proceed, or the ion can be released, and another can be loaded. This procedure can be repeated until the ion is found to be in the $^2P_{1/2}$ state. Once in the $^2P_{1/2}$ state, a particular $|F, m_F\rangle$ sublevel can be prepared using an optical pumping scheme.

For reference, following sympathetic cooling [42] and QLS [43], clock operation with an accuracy of $\Delta\nu/\nu = 2.2 \times 10^{-17}$ was recently demonstrated in B-like Ar^{13+} [44]. In that work, the main contribution to systematic uncertainty was the time-dilation shift from a technical excess micromotion (EMM) of the ion in the trap [44]. This type of EMM is typically due to trap imperfections introduced during the manufacturing process and can be reduced to a level of 10^{-19} by using a trap with low residual rf fields [45,46]. The time dilation shift due to the secular ion motion can be reduced to a low 10^{-18} or below by operating the clock near the motional ground state [40,47]. This can be accomplished by the use of sub-Doppler cooling (ground-state cooling) before clock interrogation, if the motional heating rates in the trap are low enough. If heating rates become problematic, periodic cooling during clock interrogation can be used to mitigate this heating. Due to the low differential polarizability of the clock transition, the Stark shifts associated with this cooling should be negligible.

The presence of blackbody radiation (BBR) at the location of the clock ion will cause an ac Stark shift on the clock levels, leading to a frequency shift in the clock transition. The BBR-induced frequency shift is given as $\Delta\nu = -(1/2h)\Delta\alpha\langle E^2_{\rm BBR}\rangle$, where $\Delta\alpha$ is the differential polarizability for a given clock transition, and $\langle E^2_{\rm BBR}\rangle = (831.9\ {\rm V/m})^2({\rm T}/300\ {\rm K})^4$, where T is the temperature of the BBR environment. The differential polarizabilities of the clock and logic transitions have been calculated in this work and are given in Table V. For the $^2P_{1/2} \to {}^2F_{7/2}$ transition at room temperature, the BBR-induced frequency shift would be $\Delta\nu/\nu \approx -2 \times 10^{-18}$. However, due to the high charge of Pr^{10+}, the trap must be operated at cryogenic temperatures, reducing its pressure to the level of 10^{-14} mbar to avoid ion losses by charge exchange with residual gas. At an adequate temperature of approximately 4 K, the BBR-induced frequency shift would be $\Delta\nu/\nu \approx -6 \times 10^{-26}$, which is effectively negligible.

The electric-quadrupole moments calculated for the excited clock and logic states are presented in Table V. Due to the nonzero electric-quadrupole moment in the excited clock states, an electric-field gradient at the location of the ion due, e.g., to the trapping potential, will lead to an electric-quadrupole shift on the clock transition. At usual trapping conditions [44], we estimate that the quadrupole shift when addressing a particular Zeeman sublevel will be on the order of 100 mHz ($\approx 3.5 \times 10^{-16}$, fractionally). This shift is approximately an order of magnitude smaller than in $^{88}Sr^+$ [48]. We expect that by averaging the shifts from all Zeeman sublevels, it should be possible to suppress its uncertainty to below 10^{-18} [48,49].

We also estimate the achievable clock instability. The noise-limited quantum projection instability for a clock based on a single Pr^{10+} ion can be estimated by assuming a Ramsey interrogation time that is equal to the lifetime of the excited $^2F_{7/2}$ state [50]. The clock instability is given as [51]

$$\sigma_y(t) = \frac{0.412}{\nu\sqrt{\tau t}}, \tag{7}$$

where ν is the clock frequency, τ is the lifetime of the excited state, and t is the averaging time. Under these conditions, we obtain $\sigma_y(t) \approx 1.3 \times 10^{-15}/\sqrt{t/{\rm s}}$. This value is comparable to state-of-the-art single-ion clocks based on Al^+ and Yb^+ [24,40] and is roughly a factor of 20 lower than the instability demonstrated in the recent Ar^{13+} clock [44]. With this frequency instability, it would be possible to perform clock comparisons at the low 10^{-18} level with approximately ten days of averaging time.

V. CONCLUSIONS AND PROSPECTS

We analyzed the prospect of developing a high-accuracy optical clock based on a Pr^{10+} ion and evaluated its potential systematic effects. Our calculations were contrasted with previous Pr^{9+} measurements and our current measurement of the Pr^{10+} the $|5s^25p\ {}^2P_{1/2}\rangle \to |5s^25p\ {}^2P_{3/2}\rangle$ transition. We find excellent agreement between theory and existing measurements.

The α sensitivity coefficient of Pr^{10+} is large and positive, $K = 22$. In particular, it is an order of magnitude larger than $K(Ar^{13+}) = 1.95$ [52]. We propose an initial comparison with a clock based on the $E3$ transition in Yb^+, which has a large negative α sensitivity ($K = -5.95$) [9,10]. Measurements of the frequency ratio of these two clocks with an accuracy of 10^{-18}, separated by an interval of one year, would set a limit on $\dot\alpha/\alpha$ at the level of 10^{-20}/yr. This outcome would be at the level of recent work in Yb^+ [11] that required almost 8 years of frequency-comparison data. With the development of an optical fiber network [53], it would be possible to include other clocks with different α sensitivities (that is, those based on Al^+, Sr, and Yb) to search for a wide range of new-physics signals [12,13]. Following the theoretical estimates from e.g., Ref. [54] and several other works, and in light of rapid advances in laser stabilization and frequency metrology techniques, we are optimistic about the tremendous potential of HCI with their extremely low polarizabilities for ultimately outperforming other clock transitions and providing a peer to the clocks based on the nuclear transition ^{229m}Th isomeric transition, which was recently laser excited in Ref. [55,56] and compared with a Sr lattice clock in Ref. [14] that is under development. Frequency comparisons of clocks based on HCI and trapped ^{229m}Th ions [51,57–59] will be sensitive to both the strong and electromagnetic interactions and undoubtedly open enormously interesting possibilities for the study of new physics, and for the establishment of ultrastable frequency references.

ACKNOWLEDGMENTS

This work is part of the "Thorium Nuclear Clock" project that has received funding from the European Research Council under the European Union's Horizon 2020 research and innovation program (Grant No. 856415). The calculations

in this work were done through the use of Information Technologies resources at the University of Delaware, specifically the high-performance Caviness and DARWIN computer clusters. This work was supported by National Science Foundation Grants No. PHY-2110102 and No. PHY-2309254, and the Office of Naval Research Grants No. N00014-22-1-2070 and No. N00014-20-1-2513. This work has received funding from the European Partnership on Metrology, co-financed by the European Union's Horizon Europe Research and Innovation Program and by the Participating States, under Grant No. 23FUN03 HIOC. This work has been supported by the Max Planck Society; the Max–Planck–Riken–PTB–Center for Time, Constants, and Fundamental Symmetries; and the German Federal Ministry of Education and Research (BMBF) through program Grant No. 13N15973 (Projekt VAUQSI).

[1] M. S. Safronova, D. Budker, D. DeMille, D. F. J. Kimball, A. Derevianko, and C. W. Clark, Rev. Mod. Phys. **90**, 025008 (2018).
[2] C. W. Chou, D. B. Hume, T. Rosenband, and D. J. Wineland, Science **329**, 1630 (2010).
[3] T. Bothwell, C. J. Kennedy, A. Aeppli, D. Kedar, J. M. Robinson, E. Oelker, A. Staron, and J. Ye, Nature (London) **602**, 420 (2022).
[4] X. Zheng, J. Dolde, V. Lochab, B. N. Merriman, H. Li, and S. Kolkowitz, Nature (London) **602**, 425 (2022).
[5] K. Beloy, M. I. Bodine, T. Bothwell, S. M. Brewer, S. L. Bromley, J.-S. Chen, J.-D. Deschênes, S. A. Diddams, R. J. Fasano, T. M. Fortier, Y. S. Hassan, D. B. Hume, D. Kedar, C. J. Kennedy, I. Khader, A. Koepke, D. R. Leibrandt, H. Leopardi, A. D. Ludlow, W. F. McGrew *et al.* [Boulder Atomic Clock Optical Network (BACON) Collaboration], Nature (London) **591**, 564 (2021).
[6] C. Sanner, N. Huntemann, R. Lange, C. Tamm, E. Peik, M. S. Safronova, and S. G. Porsev, Nature (London) **567**, 204 (2019).
[7] R. Lange, N. Huntemann, J. M. Rahm, C. Sanner, H. Shao, B. Lipphardt, C. Tamm, S. Weyers, and E. Peik, Phys. Rev. Lett. **126**, 011102 (2021).
[8] T. Rosenband, D. B. Hume, P. O. Schmidt, C. W. Chou, A. Brusch, W. H. Oskay, R. E. Drullinger, F. T. M., J. E. Stalnaker, S. A. Diddams, W. C. Swann, N. R. Newbury, W. M. Itano, D. J. Wineland, and J. C. Bergquist, Science **319**, 1808 (2008).
[9] R. M. Godun, P. B. R. Nisbet-Jones, J. M. Jones, S. A. King, L. A. M. Johnson, H. S. Margolis, K. Szymaniec, S. N. Lea, K. Bongs, and P. Gill, Phys. Rev. Lett. **113**, 210801 (2014).
[10] N. Huntemann, B. Lipphardt, C. Tamm, V. Gerginov, S. Weyers, and E. Peik, Phys. Rev. Lett. **113**, 210802 (2014).
[11] M. Filzinger, S. Dörscher, R. Lange, J. Klose, M. Steinel, E. Benkler, E. Peik, C. Lisdat, and N. Huntemann, Phys. Rev. Lett. **130**, 253001 (2023).
[12] A. D. Ludlow, M. M. Boyd, J. Ye, E. Peik, and P. O. Schmidt, Rev. Mod. Phys. **87**, 637 (2015).
[13] M. G. Kozlov, M. S. Safronova, J. R. Crespo López-Urrutia, and P. O. Schmidt, Rev. Mod. Phys. **90**, 045005 (2018).
[14] C. Zhang, T. Ooi, J. S. Higgins, J. F. Doyle, L. von der Wense, K. Beeks, A. Leitner, G. A. Kazakov, P. Li, P. G. Thirolf, T. Schumm, and J. Ye, Nature (London) **633**, 63 (2024).
[15] J. C. Berengut, V. A. Dzuba, and V. V. Flambaum, Phys. Rev. Lett. **105**, 120801 (2010).
[16] J. C. Berengut, V. A. Dzuba, V. V. Flambaum, and A. Ong, Phys. Rev. Lett. **106**, 210802 (2011).
[17] J. C. Berengut, V. A. Dzuba, V. V. Flambaum, and A. Ong, Phys. Rev. A **86**, 022517 (2012).
[18] M. S. Safronova, V. A. Dzuba, V. V. Flambaum, U. I. Safronova, S. G. Porsev, and M. G. Kozlov, Phys. Rev. Lett. **113**, 030801 (2014).
[19] A. Ong, J. C. Berengut, and V. V. Flambaum, Optical transitions in highly charged ions for detection of variations in the fine-structure constant, in *Fundamental Physics in Particle Traps*, edited by W. Quint and M. Vogel (Springer, Berlin, Heidelberg, 2014), pp. 293–314.
[20] V. A. Dzuba and V. V. Flambaum, Hyperfine Interact. **236**, 79 (2015).
[21] S. Schiller, Phys. Rev. Lett. **98**, 180801 (2007).
[22] N. S. Oreshkina, S. M. Cavaletto, N. Michel, Z. Harman, and C. H. Keitel, Phys. Rev. A **96**, 030501(R) (2017).
[23] P. O. Schmidt, T. Rosenband, C. Langer, W. M. Intano, J. C. Bergquist, and D. J. Wineland, Science **309**, 749 (2005).
[24] N. Huntemann, C. Sanner, B. Lipphardt, C. Tamm, and E. Peik, Phys. Rev. Lett. **116**, 063001 (2016).
[25] H. Bekker, A. Borschevsky, Z. Harman, C. H. Keitel, T. Pfeifer, P. O. Schmidt, J. R. Crespo López-Urrutia, and J. C. Berengut, Nat. Commun. **10**, 5651 (2019).
[26] S. G. Porsev, U. I. Safronova, M. S. Safronova, P. O. Schmidt, A. I. Bondarev, M. G. Kozlov, I. I. Tupitsyn, and C. Cheung, Phys. Rev. A **102**, 012802 (2020).
[27] M. S. Safronova, M. G. Kozlov, W. R. Johnson, and D. Jiang, Phys. Rev. A **80**, 012516 (2009).
[28] C. Cheung, M. Safronova, and S. Porsev, Symmetry **13**, 621 (2021).
[29] S. G. Porsev and A. Derevianko, Phys. Rev. A **73**, 012501 (2006).
[30] I. I. Tupitsyn, M. G. Kozlov, M. S. Safronova, V. M. Shabaev, and V. A. Dzuba, Phys. Rev. Lett. **117**, 253001 (2016).
[31] M. G. Kozlov, M. S. Safronova, S. G. Porsev, and I. I. Tupitsyn, Phys. Rev. A **94**, 032512 (2016).
[32] M. S. Safronova, V. A. Dzuba, V. V. Flambaum, U. I. Safronova, S. G. Porsev, and M. G. Kozlov, Phys. Rev. A **90**, 042513 (2014).
[33] N. J. Stone, At. Data Nucl. Data Tables **90**, 75 (2005).
[34] V. A. Dzuba, M. G. Kozlov, S. G. Porsev, and V. V. Flambaum, Zh. Eksp. Teor. Fiz. **114**, 1636 (1998) [Sov. Phys. JETP **87** 885, (1998)].
[35] J. R. Crespo López-Urrutia, J. Braun, G. Brenner, H. Bruhns, C. Dimopoulou, I. N. Draganić, D. Fischer, A. J. González Martínez, A. Lapierre, V. Mironov, R. Moshammer, R. S. Orts, H. Tawara, M. Trinczek, and J. Ullrich, J. Phys.: Conf. Ser. **2**, 42 (2004).
[36] M. A. Levine, R. E. Marrs, J. R. Henderson, D. A. Knapp, and M. B. Schneider, Phys. Scr. **1988**, 157 (1988).

[37] B. M. Penetrante, J. N. Bardsley, M. A. Levine, D. A. Knapp, and R. E. Marrs, Phys. Rev. A **43**, 4873 (1991).
[38] H. Bekker, C. Hensel, A. Daniel, A. Windberger, T. Pfeifer, and J. R. Crespo López-Urrutia, Phys. Rev. A **98**, 062514 (2018).
[39] P. Tremblay, A. Michaud, M. Levesque, S. Thériault, M. Breton, J. Beaubien, and N. Cyr, Phys. Rev. A **42**, 2766 (1990).
[40] S. M. Brewer, J.-S. Chen, A. M. Hankin, E. R. Clements, C. W. Chou, D. J. Wineland, D. B. Hume, and D. R. Leibrandt, Phys. Rev. Lett. **123**, 033201 (2019).
[41] A. L. Banducci, A. S. Naing, J. B. VanArsdale, and S. M. Brewer (unpublished).
[42] L. Schmöger, O. O. Versolato, M. Schwarz, M. Kohnen, A. Windberger, B. Piest, S. Feuchtenbeiner, J. Pedregosa-Gutierrez, T. Leopold, P. Micke, A. K. Hansen, T. M. Baumann, M. Drewsen, J. Ullrich, P. O. Schmidt, and J. R. Crespo López-Urrutia, Science **347**, 1233 (2015).
[43] P. Micke, T. Leopold, S. A. King, E. Benkler, L. J. Spieß, L. Schmöger, M. Schwarz, J. R. Crespo López-Urrutia, and P. O. Schmidt, Nature (London) **578**, 60 (2020).
[44] S. A. King, L. J. Spieß, P. Micke, A. Wilzewski, T. Leopold, E. Benkler, R. Lange, N. Huntemann, A. Surzhykov, V. A. Yerokhin, J. R. Crespo López-Urrutia, and P. O. Schmidt, Nature (London) **611**, 43 (2022).
[45] J. Keller, H. L. Partner, T. Burgermeister, and T. E. Mehlstäubler, J. Appl. Phys. **118**, 104501 (2015).
[46] J. Keller, T. Burgermeister, D. Kalincev, A. Didier, A. P. Kulosa, T. Nordmann, J. Kiethe, and T. E. Mehlstäubler, Phys. Rev. A **99**, 013405 (2019).
[47] J.-S. Chen, S. M. Brewer, C. W. Chou, D. J. Wineland, D. R. Leibrandt, and D. B. Hume, Phys. Rev. Lett. **118**, 053002 (2017).
[48] P. Dubé, A. A. Madej, Z. Zhou, and J. E. Bernard, Phys. Rev. A **87**, 023806 (2013).
[49] P. Dubé, A. A. Madej, J. E. Bernard, L. Marmet, J.-S. Boulanger, and S. Cundy, Phys. Rev. Lett. **95**, 033001 (2005).
[50] W. M. Itano, J. C. Bergquist, J. J. Bollinger, J. M. Gilligan, D. J. Heinzen, F. L. Moore, M. G. Raizen, and D. J. Wineland, Phys. Rev. A **47**, 3554 (1993).
[51] E. Peik, T. Schneider, and C. Tamm, J. Phys. B: At., Mol. Opt. Phys. **39**, 145 (2006).
[52] Y.-M. Yu, B. K. Sahoo, and B.-B. Suo, Front. Phys. **11**, 1104848 (2023).
[53] J. B. VanArsdale, M. K. Deutch, M. Lombardi, G. Nelson, J. Sherman, J. Spice, W. C. Yates, D. C. Yost, and S. M. Brewer, Opt. Lett. **49**, 2545 (2024).
[54] V. I. Yudin, A. V. Taichenachev, and A. Derevianko, Phys. Rev. Lett. **113**, 233003 (2014).
[55] J. Tiedau, M. V. Okhapkin, K. Zhang, J. Thielking, G. Zitzer, E. Peik, F. Schaden, T. Pronebner, I. Morawetz, L. T. De Col, F. Schneider, A. Leitner, M. Pressler, G. A. Kazakov, K. Beeks, T. Sikorsky, and T. Schumm, Phys. Rev. Lett. **132**, 182501 (2024).
[56] R. Elwell, C. Schneider, J. Jeet, J. E. S. Terhune, H. W. T. Morgan, A. N. Alexandrova, H. B. T. Tan, A. Derevianko, and E. R. Hudson, Phys. Rev. Lett. **133**, 013201 (2024).
[57] E. Peik and C. Tamm, Europhys. Lett. **61**, 181 (2003).
[58] P. V. Bilous, H. Bekker, J. C. Berengut, B. Seiferle, L. von der Wense, P. G. Thirolf, T. Pfeifer, J. R. Crespo López-Urrutia, and A. Pálffy, Phys. Rev. Lett. **124**, 192502(R) (2020).
[59] E. Peik, T. Schumm, M. S. Safronova, A. Pálffy, J. Weitenberg, and P. G. Thirolf, Quantum Sci. Technol. **6**, 034002 (2021).